ACS APPLIED MATERIALS & INTERFACES

Research Article

www.acsami.org

Evolution of a Mesoporous Bioactive Glass Scaffold Implanted in Rat Femur Evaluated by ^{45}Ca Labeling, Tracing, and Histological Analysis

Baiyan Sui,[†] Gaoren Zhong,[‡] and Jiao Sun*[,†]

[†]Shanghai Biomaterials Research & Testing Center, Shanghai Key Laboratory of Stomatology, Ninth People's Hospital, Shanghai Jiaotong University School of Medicine, Shanghai 200023, China

[‡]School of Pharmacy, Fudan University, Shanghai 201203, China

ABSTRACT: Mesoporous bioactive glass (MBG) as a biodegradable scaffold with a nanostructure has attracted significant attention. However, the in vivo evolution of MBG, which includes in situ degradation, the local effect induced by degradation, and the disposition of degradation products, remains unclear. In this study, we performed in situ labeling and synthesis of an MBG scaffold for the first time using $^{45}CaCl_2$. The obtained ^{45}Ca-MBG scaffolds possessed a mesoporous−macroporous cross-linked structure. These ^{45}Ca-MBG scaffolds were implanted in critical-sized rat femur defects (3 × 3 mm) for 1 day and for 1, 4, 8, and 12 weeks and analyzed by isotopic quantitative tracing. The results illustrated that the MBG scaffolds gradually degraded over time and persisted at a local level of approximately 9.63% at week 12. This finding suggests that only a very small amount of MBG-released calcium ions may have been transformed into calcium components of the new bone matrix. The research also confirmed that the active ingredients derived from the degradation of MBG scaffolds could actively regulate the mRNA expression levels of osteoblast-related genes in rat bone marrow-derived mesenchymal stem cells (rBMSCs) and promote bone regeneration in vivo. Moreover, through isotopic tracing of the entire body, ^{45}Ca, which disappeared in situ after implantation, could be detected in the heart, lungs, spleen, kidneys, intestines, and brain via the blood and was mainly accumulated in distal bone tissue, including the radius and cranium. However, ^{45}Ca radioactivity in the body tissues significantly decreased or disappeared after 12 weeks. Systemic toxicological studies on MBG scaffolds demonstrated the degradation products that spread to major organs did not cause abnormal histopathological changes. The above discoveries comprehensively address crucial issues regarding the application of MBG in vivo, and these findings provide a scientific basis for introducing a material with mesoporous structure into clinical applications.

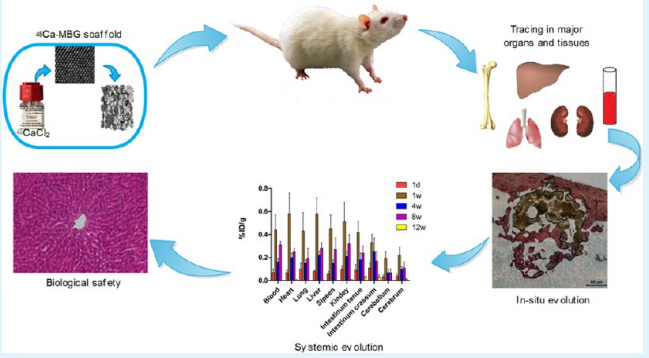

KEYWORDS: *mesoporous bioactive glass, in vivo evolution, ^{45}Ca labeling, tissue distribution, bone implantation, degradation products*

INTRODUCTION

Recently, because of its excellent properties such as high specific surface area, capacity for controlled drug/protein delivery, and greatly improved biological activity, mesoporous bioactive glass (MBG) has been considered as a potential scaffold for bone repair and drug loading.[1−6] MBG with a composition of $80SiO_2−15CaO−5P_2O_5$ (mol %) shows strong biological mineralization activity in vitro.[7−10] Despite being a great potential candidate for mesoporous−porous scaffold fabrication, the biological evolution and degradation process of MBG scaffolds in vivo are still unclear, with many important questions unanswered. Namely, what kind of role do the nanostructure and the ion-release characteristics of MBG scaffolds play in their biological effects? Can the local degradation process effectively stimulate autologous tissue formation simultaneously? Are the ingredients resulting from the evolution of MBG scaffolds involved in local or systemic metabolism? Additionally, does MBG evolution adversely affect major body organs? These questions are directly related to the benefits and risks of the in vivo clinical application of MBG and must be answered prior to use in translational medicine.

To reveal the nature of MBG evolution in vivo, both local and systemic evolution after scaffold implantation should be considered. The first consideration is the biological effect of the local evolution induced by ions released from MBG. Our previous studies found that a calcium silicate composite scaffold effectively enhanced the expression of osteogenic genes and proteins by releasing calcium and silicon ions in vitro;[11] the degradation products released from MBG scaffolds have been reported to play the same role.[2,12] However, little information has been disclosed on the relationship between the osteogenic effects of MBG scaffolds and their released ions in vivo, and evidence addressing the questions about MBG scaffolds is still lacking.

Received: December 10, 2013
Accepted: January 20, 2014
Published: January 20, 2014

   dx.doi.org/10.1021/am4056886 | *ACS Appl. Mater. Interfaces* 2014, 6, 3528−3535

Another important aspect that must be paid attention to is the destination of degradation products and the systemic effects induced by these products during the evolution of MBG scaffolds. To clarify this point, an effective technique for labeling MBG scaffolds must be established to resolve the problem of long-term quantitative tracking in vivo. That is, it is vital to trace the distribution and accumulation of degradation products in body tissues and organs throughout the entire scaffold degradation period. However, at present, there is no research in this sphere. Radiolabeling has the potential for long-term quantitative tracing of materials in vivo and can also exclude the possibility of interference by endogenous elements such as Ca and P, whereas ICP measurement is susceptible to interference by endogenous elements in vivo.[13,14] In 2011, Ann Wennerberg applied radionuclide calcium (^{45}Ca) to the in situ labeling of a nanometer-sized hydroxyl phosphorite layer on the surface of titanium and utilized autoradiography for qualitative analysis of changes in the radioactivity of the implant.[15] However, the study did not include local quantitative tracing. The calcium content of MBG is also a very important factor because decreasing the amount of CaO in a SiO_2−CaO-P_2O_5 system favors the formation of hexagonal rather than cubic phases in MBG nanostructures.[16,17] Therefore, the present research used in situ labeling of MBG scaffolds with ^{45}Ca for the objective and accurate assessment of the in vivo evolution of mesoporous−porous scaffolds with the composition $80SiO_2$−$15CaO$−$5P_2O_5$, which avoided the destruction of the mesoporous structure and changes in the physical and chemical properties of MBG scaffolds that result from adopting an exogenous radionuclide or fluorescent marker.[18,19]

In this study, MBG scaffolds were synthesized using ^{45}Ca-$(NO_3)_2{\cdot}4H_2O$, which ensured accurate nanostructures and compositions, and these scaffolds were implanted in the femoral condyles of rats. The degradation products of the MBG scaffolds were traced at different time points, including 1 day and 1, 4, 8, and 12 weeks after implantation. We then analyzed the distribution and local and systemic accumulation of ^{45}Ca in major tissues and organs to reveal fully the in vivo evolution. Furthermore, through quantitative histological analysis, we evaluated the local evolution process involving the degradation of materials and the capacity for new bone formation at 4, 8, and 12 weeks after implantation of MBG scaffolds in the same model. The results combined with isotope tracer research demonstrated the contributions of the nanostructure, the degradation products, and the associated microenvironment to ossification. The microenvironment was also mimicked using extracts from the MBG scaffolds, and the capability of this ionic environment to alter rat bone marrow-derived mesenchymal stem cell (rBMSC) osteogenic differentiation was preliminarily investigated, particularly at the gene level. Finally, whether the degradation products caused a systemic subacute (subchronic) toxicity reaction was evaluated, and the potential for future clinical applications of MBG scaffolds was comprehensively assessed.

EXPERIMENTAL SECTION

Radiolabeling of MBG Scaffolds with ^{45}Ca. A test tube was coated with 100 μL of $CaCl_2$ reagent (10 mg/mL in deionized water) and was subsequently dried with a gentle stream of nitrogen for 30−60 min. ^{45}Ca-MBG scaffolds were prepared by adding ^{45}Ca (PerkinElmer, $^{45}CaCl_2$, 74 MBq) to a solution of $NaNO_3$ in the coated test tube and stirring at room temperature for 1 h, resulting in $^{45}Ca(NO_3)_2{\cdot}4H_2O$, which was used to synthesize scaffolds using P123 and polyurethane sponges. Briefly, 4 g of P123 (MW = 5800, Sigma), 1.4 g of $Ca(NO_3)_2{\cdot}4H_2O$ (including $^{45}Ca(NO_3)_2{\cdot}4H_2O$), 6.7 g of tetraethyl orthosilicate (TEOS, 98%, Sigma), 0.73 g of triethyl phosphate (TEP, 99.8%, Sigma), and 1.0 g of 0.5 M HCl were dissolved in 60 g of ethanol (Si/Ca/P = 80:15:5, molar ratio) and then stirred at room temperature for 24 h. The polyurethane sponges were cleaned, completely immersed in this solution for 15 min, and then transferred to a Petri dish. Excess gel was squeezed out, and the sponges were dried under a fume hood in air at room temperature for 24 h. This procedure was repeated six times to control the large-pore porosity of the scaffolds. Once the samples were completely dried, they were calcined at 700 °C for 6 h to obtain the final ^{45}Ca-MBG scaffolds. The radioactivity per scaffold was 185 kBq for the ^{45}Ca-MBG scaffold (3 mm in length and 3 mm in diameter). Nonradioactive MBG scaffolds were synthesized using the same process without adding $^{45}Ca(NO_3)_2{\cdot}4H_2O$ (φ 3 × 3 mm).

Characterization of MBG Scaffolds. The surface morphology of the MBG scaffolds was analyzed by scanning electron microscopy (SEM), and the inner microstructure was confirmed by small-angle X-ray diffraction (SAXRD) and transmission electron microscopy (TEM). The surface area, pore-size distribution, and pore volume were measured using Brunauer−Emmett−Teller (BET) and Barrett−Joyner−Halenda (BJH) analyses by N_2 adsorption−desorption isotherms. The ^{45}Ca-MBG scaffolds were individually immersed in simulated body fluid (SBF) at 37 °C, and the supernatant was extracted and filtered at seven time points (1, 3, and 6 h as well as 1, 3, 6, and 10 days). The radioactivity of the filtrate was analyzed by liquid scintillation counting (LSC), and the in vitro release rate (%) of ^{45}Ca ions from the ^{45}Ca-MBG scaffold was calculated.

Implantation of ^{45}Ca-MBG Scaffolds in Rat Femur. The Animal Care and Experiment Committee of the Ninth People's Hospital affiliated with the School of Medicine, Shanghai Jiao Tong University, approved the experimental protocol. Twenty-five healthy Sprague−Dawley rats were used in this study. All animals weighed between 240 and 250 g. The rats were divided randomly into five groups according to the presumed measurement time, and each group contained five rats. The rats were anesthetized with an intraperitoneal injection of 3% pentobarbital sodium (1.0 mL/kg). Under strict sterile conditions, a critical-sized defect with a diameter of 3 mm and a depth of 3 mm was made in the bilateral femoral condyles using a hand drill. The defect was orientated perpendicular to the long axis of the femur. The ^{45}Ca scaffold was implanted, and the muscles and the skin were sutured. The rats were euthanized 1 day or 1, 4, 8, and 12 weeks after implantation and used for isotopic tracing.

Local and Systemic Isotopic Tracing of ^{45}Ca-MBG Scaffolds. The blood, femur, radius, cranium, and organs, including the heart, lungs, liver, spleen, kidneys, intestinum tenue, intestinum crassum, cerebrum, and cerebella, were harvested and weighed after 1 day or after 1, 4, 8, and 12 weeks postimplantation. Samples were dissected and dissolved with 1 mL of perchloric acid and 1 mL of hydrogen peroxide in a 60 °C water bath for 2 h. Then, 3 mL of Hionic-Fluor liquid scintillation cocktail was added to each 100 μL aliquot of the dissolved samples, and the solution was shaken for 60 s. Measurements were taken using a Wallac 1450 Microbeta (Wallac, Finland). The radioactivity of the samples was determined using the following equation

$$A_0 = \frac{A_t}{e^{-0.963t/t_{1/2}}}$$

where A_t is the actual radioactivity, A_0 is the radioactivity when the ^{45}Ca-MBG scaffolds were synthesized, $t_{1/2}$ is the half-life of ^{45}Ca (163 days), and t is the time interval between A_t and A_0. The local degradation and systemic evolution are expressed as the percentage of the implanted dose per gram of tissue (%ID/g).

Analysis of MBG Scaffold Extracts. Extracts of the porous MBG scaffolds were prepared according to the International Organization for Standardization' requirements (ISO 10993-12).[20] The ratio of the scaffold-to-medium was 100 mg/mL. The scaffolds were incubated for 24 h at 37 °C in low-glucose Dulbecco's modified Eagle's medium (L-DMEM, HyClone, USA). The extracts were analyzed using inductively

Table 1. Primers Used for Real-Time PCR

target gene	forward primer sequence (5′−3′)	reverse primer sequence (5′−3′)
GAPDH	ATGCCTTGTTCTCCTCTTACTGGA	CTTTCTGCTGCTAATGTTCTTGACC
RUNX-2	GCCGGGAATGATGAGAACTA	GAGGCAGAAGTCAGAGGTGG
ALP	CCTAGACACAAGCACTCCCACTA	GTCAGTCAGGTTGTTCCGATTC
OCN	GTGCCGTCCATACTTTCG	GACCACATTGGCTTCCAG

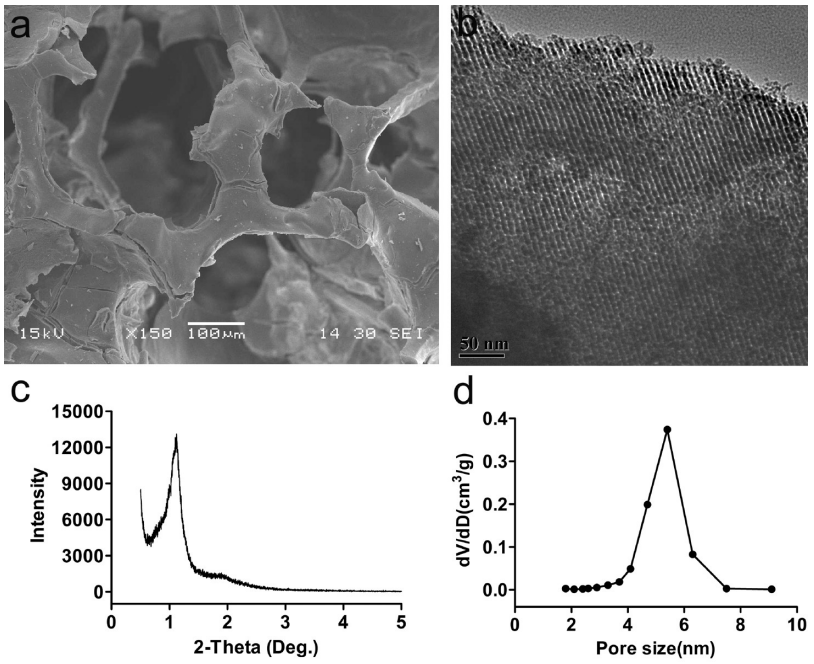

Figure 1. SEM (a), TEM (b), and SAXRD (c) analyses and mesopore size distribution (d) of the MBG scaffold.

coupled plasma optical emission spectroscopy (ICP-OES; VISTAP-RO, Agilent, USA) to determine the elemental concentrations of calcium, silicon, and phosphorus (Ca, Si, and P, respectively). Changes in the pH value of the extracts were detected using a pH meter (Denver UB-7, YaoHua Co., China).

Osteogenic Effect of MBG Scaffolds in Vitro. rBMSCs were obtained and cultured from the femora of 4 week old Sprague−Dawley rats using the protocol described in our previous study.[21] Cells from the second and third passages were used for the following experiments. The cell viability was quantitatively assessed with a 3-(4,5-dimethylthiazol-2-yl)-2,5-diphenyltetrazolium bromide (MTT) colorimetric assay.[8] The osteoblastic gene transcription of ALP, RunX-2, and OCN was detected by real-time polymerase chain reaction (PCR). Briefly, rBMSCs were cultured in the extracts of the MBG scaffolds for 3 and 10 days. Total RNA was isolated using TRIzol reagent (Invitrogen, USA), and 1.0 μg of the RNA was reverse transcribed into complementary DNA (cDNA) using the Prime-Script first-strand cDNA synthesis kit (TaKaRa, Japan) according to the manufacturer's instructions. The expression was quantified by a Bio-Rad sequence-detection system (MyiQ2, USA) using a real-time PCR kit (SYBR Premix Ex Taq, TaKaRa). The gene-expression levels were normalized to the levels of the housekeeping gene GAPDH. The primers for the selected genes are shown in Table 1.

Osteogenesis and Degradation of MBG Scaffolds in Situ with Quantitative Histological Analysis. The experimental protocol was approved by the Animal Care and Experiment Committee of the Ninth People's Hospital affiliated with the School of Medicine, Shanghai Jiao Tong University. Fifteen healthy Sprague−Dawley rats were used in this study. All animals weighed between 245 and 250 g. The rats were randomly divided into three groups of five rats each according to the presumed measurement time. The surgical procedures were performed under general anesthesia, as described above. An MBG scaffold was implanted into the unilateral femoral condyle of a rat, and the empty bony defects served as the control. The animals were euthanized for analysis 4, 8, and 12 weeks after implantation, and the femora were removed for histological analysis. The harvested samples were fixed in 10% neutral-buffered formaldehyde (pH 7.2) for 2 weeks and dehydrated in a graded series of ethanol. Subsequently, the samples were embedded in polymethylmethacrylate (PMMA) without decalcification, sectioned, and then stained with Van Gieson's picric acid-fuchsin. Each group contained five samples, and three sections of each sample were used for histomorphometric analysis with a semiautomatic image-analysis system (Bioquant Osteo II). The percentage of newly formed bone (NB) and the degradation rate of the material (DR) were calculated according to the following equations:

$$\mathrm{NB}\,(\%) = (\text{area of newly formed bone in the 3 mm diameter defect} / \text{total area of the 3 mm diameter defect})100$$

$$\mathrm{DR}\,(\%) = [1 - (\text{residual material area} - \text{initial material area})]100$$

Assessment of Systemic Toxicity Caused by MBG Degradation Products. The systemic toxicity, which included histopathology, hematology, and clinical chemistry, was evaluated according to the International Organization for Standardization (ISO 10993-11) standards at 4 and 12 weeks after implantation of the MBG scaffolds.[22] The histopathology of 26 organs, including the liver, spleen, kidneys, lungs, and heart, was observed under an optical microscope. The following hematological parameters were measured using a hematological auto analyzer (Coulter T540 hematology system; Beckman Coulter, Inc.): white blood cell count (WBC), neutrophil (NEU), lymphocyte (LYM), monocyte (MONO), erythrocyte, and platelet counts, and hemoglobin. Standard spectrophotometric methods via the Cobas Integra 400 Plus automatic biochemistry analyzer (Roche) were used to measure the following clinical biochemical parameters: alanine aminotransferase, aspartate aminotransferase (AST), alkaline

phosphatase, total bile acid, blood urea nitrogen, cholesterol, triglyceride, uric acid, creatine kinase, high-density lipoprotein, and low-density lipoprotein.

Statistical Analysis. The data are expressed as the mean ± standard deviation (SD). Statistical analyses were performed using SPSS software (v 12.0; IBM Corporation, USA), and statistical comparisons were analyzed using a one-way ANOVA. Differences were considered statistically significant when $p < 0.05$.

RESULTS AND DISCUSSION

Their bioactivity and capacity for controlled drug delivery, which are due to the composition and highly ordered mesoporous arrangement of the cavities present in nanostructured materials, make MBG a good candidate for the manufacturing of three-dimensional scaffolds for bone tissue engineering.[23−25] However, to make MBG eventually applicable in the clinic, the evolution of MBG in vivo must be systematically characterized. The evolution of MBG entails the local degradation of scaffolds, MBG-induced biological effects, including osteogenesis and angiogenesis, the disappearance or reuse of the degradation products, including distribution and accumulation, and the risks of the application, which might be caused by systemic distribution after MBG scaffold implantation.

Establishment of a Labeling Technique for Assessing ^{45}Ca-MBG Scaffold Evolution Process. MBG is a biodegradable mesoporous material, and the assessment of its degradation products in vivo is crucial for evaluating the effects and risks of the final application of MBG scaffolds. To understand the evolution process, the problem of labeling needs to be solved first. A labeling technique that can not only maintain the nanostructure of MBG but also ensure effective tracing during the degradation of scaffolds must be established. Unfortunately, there are no reports related to a labeling technique for MBG scaffolds that can fulfill these requirements. The present study first employs an isotopic labeling technique that can provide quantitative analysis that combines accurate positioning with high sensitivity. When using MBG with a $SiO_2-CaO-P_2O_5$ composition, Ca was selected as the tracer element because the half-life of calcium isotopes (^{45}Ca) is 163 days, which is longer than that of the isotopes of other ions (Si and P) released by MBG. As a result, Ca is more suitable for characterizing scaffold degradation and fulfilling the objective of a long-term quantitative study in vivo. The results indicated that ^{45}Ca, an effective systemic tracer element, was successfully introduced into the mesoporous structure network of the MBG scaffold by converting $^{45}CaCl_2$ into $^{45}Ca(NO_3)_2{\cdot}4H_2O$. The scaffold had a highly porous structure, with a pore size ranging from approximately 300 to 500 μm (Figure 1a), and a well-ordered mesoporous structure (pore size: approximately 6.40 nm, Figure 1b,d). The radioactivity of the ^{45}Ca in MBG scaffold remained at a level of 84.32% after soaking for 10 days in vitro, which demonstrated that the ^{45}Ca ions from the synthetic, radioactive MBG scaffold did not exhibit burst release (Figure 2).

Evolution of MBG Scaffolds in Situ. Following the successful synthesis of ^{45}Ca-MBG scaffolds, we first inspected the in situ evolution of the MBG scaffolds in vivo. Through isotope tracing and quantitative histological analysis, the degradation process and biological effect of MBG scaffolds in situ were studied. The local evolution of the ^{45}Ca-MBG scaffolds after implantation in femoral condyles confirmed an obvious time dependence of this process, as reflected by a decrease in the ^{45}Ca radioactivity (Figure 3). The remaining percentage of ^{45}Ca at the implantation site was 96.89 ± 1.22% on the first day after implantation and decreased to 9.63 ± 1.63% by the 12th week, demonstrating significant degradation of the MBG scaffolds. This phenomenon was influenced by the structural features of MBG, including nanostructures and a large specific surface area (343.444 m^2/g), which increase the contact area with body fluids and accelerate the ion release and degradation of the scaffolds.[26] However, it is unclear whether the ionic products released from this degradation are directly involved in new bone formation. There is no valid experiment to test and verify this issue, although previous studies have speculated that 25% of the released Ca could theoretically be involved in mineralization processes for a β-TCP scaffold with a given Ca content.[27] The present research found that the remaining percentage of radioactivity that was detected in local bone was only approximately 9.63% at week 12, and the quantitative histological analysis indicated that the scaffold was almost completely degraded at this time (95.98 ± 1.06%; Figure 6b). These findings indicate that only a small amount of Ca ions released during degradation was involved new bone formation and was directly converted into matrix.

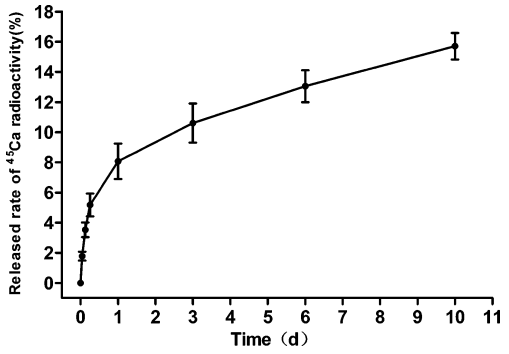

Figure 2. ^{45}Ca release from ^{45}Ca-MBG scaffold on day 10 in vitro.

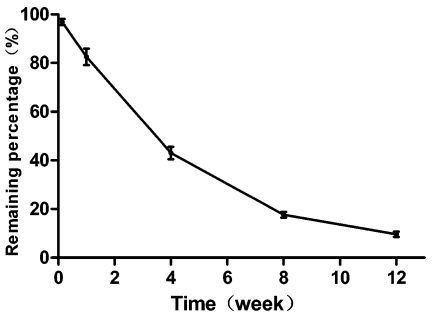

Figure 3. Remaining percentage of ^{45}Ca radioactivity at the implantation site 1 day and 1, 4, 8, and 12 weeks postimplantation.

To gain insight into osteogenic potential of the ionic products released from the mesoporous−porous scaffold, we designed a coculture system including scaffold extracts and rBMSCs, which mimicked the in vivo microenvironment. The result showed that immersion of rBMSCs in extracts of the MBG scaffolds for 3 and 10 days significantly enhanced the mRNA levels of the RUNX-2, ALP, and OCN genes, which are related to osteogenesis (Figure 4b−d). RUNX-2 is a well-known, crucial osteoblast transcription factor, and ALP and OCN are key markers of early-stage mineralization and osteogenic differentiation. The enhanced mRNA levels may

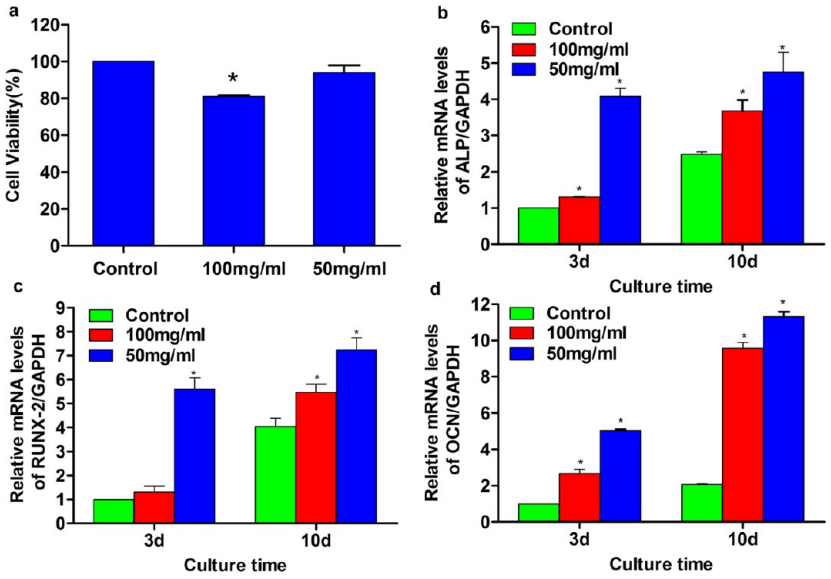

Figure 4. Effect of different extracts on cell viability. (a) Gene-expression profile of the osteogenic differentiation-related genes of rBMSCs cultured with different extracts: (b) ALP, (c) RUNX-2, and (d) OCN. Cells cultured in L-DMEM were set as the control group. * indicates results that are significantly different from the result of the L-DMEM group ($p < 0.05$).

Table 2. Measured Concentration (±SD) (mg/L) and pH

	Si	Ca	P	pH
L-DMEM	<0.02	89.18 ± 1.7	45.77 ± 1.2	7.24 ± 0.06
50 mg/mL	83.8 ± 4.8	127.79 ± 5.8	32.30 ± 2.1	7.97 ± 0.07
100 mg/mL	141.47 ± 2.7	248.58 ± 10.3	41.15 ± 5.3	8.72 ± 0.04

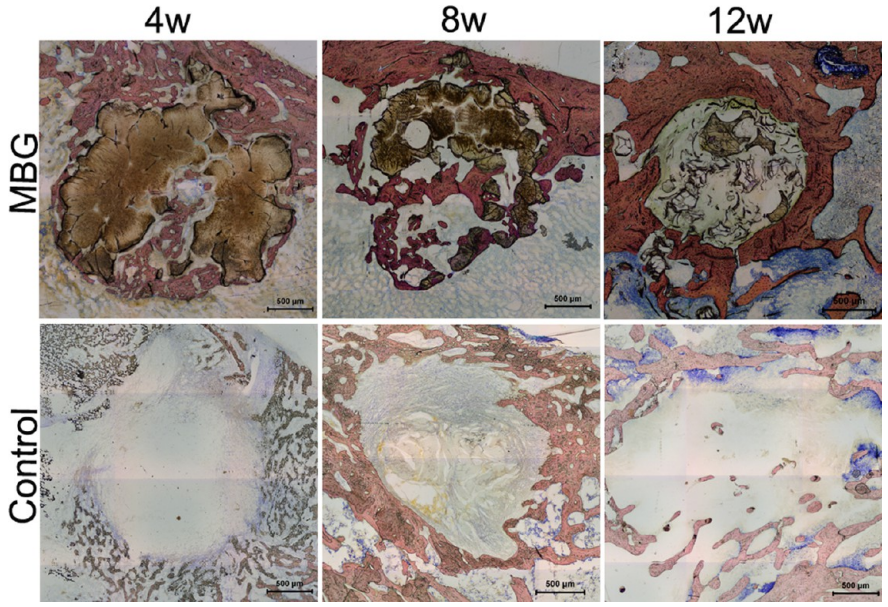

Figure 5. New bone formation and material degradation in MBG scaffolds 4, 8, and 12 weeks after implantation (Van Gieson's picric acid-fuchsin staining). Red, green, and brown represent the newly formed bone, fibrous tissue, and residual material, respectively. The scale bar is 500 μm. Negative groups were used as the control.

have been induced by the ions released from the scaffolds, directly inducing the osteogenic differentiation of the rBMSCs. ICP-OES analysis further confirmed that these ions were mainly Si and Ca (Table 2). It has been shown that Si and Ca ions are capable of promoting osteogenic gene expression.[28,29] Moreover, the mRNA expression level of osteoblast-related genes in the 50 mg/mL extract was higher than that in the 100 mg/mL extract, which is because the 100 mg/mL extract leached more Ca ions and caused the pH value of the extract to increase (pH 8.7), changing the extracellular microenvironment and consequently affecting the differentiation of the rBMSCs and reducing mRNA levels.

Because it was proved that ionic products from MBG scaffolds play a significant role in promoting bone formation, it

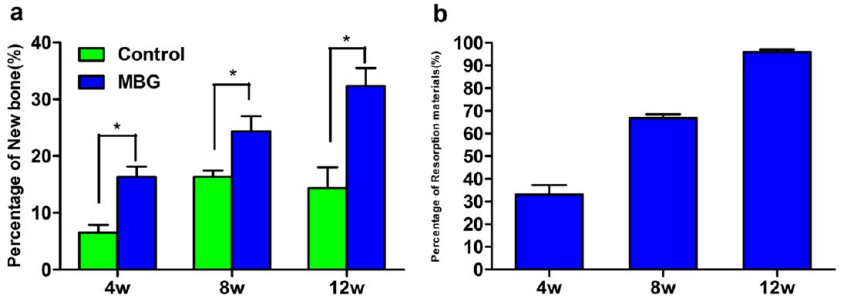

Figure 6. Histomorphometric analysis of the percentage of newly formed bone (a) and the percentage of degraded materials (b) at different time points after implantation. * indicates results that are significantly different from the result of the control group ($p < 0.05$).

was necessary to study further how the scaffolds mediated local biological effects. The histological analysis (Figure 5) showed that the MBG scaffolds were adsorbed and that new bone invaded the scaffolds, from the edge to the center, from weeks 4 to 12 postimplantation. Lamellar bone and Haversian canals were detected in the MBG scaffolds after 12 weeks, and the scaffolds had degraded substantially. The results of the quantitative analysis also indicated that the MBG scaffolds exerted an osteostimulatory effect and promoted new bone formation (Figure 6). These findings demonstrate that the MBG scaffolds can effectively stimulate bone formation in the evolution process. The nanostructure system not only provides a high surface area and pore volume (343.444 m^2/g and 0.565 cm^3/g, respectively) but also allows easier ionic exchange with the surrounding medium by increasing the mass transport and diffusion processes. Meanwhile, the extracellular microenvironment, which was formed by the soluble Si and Ca ions released during the degradation process, effectively induced the osteogenic differentiation of rBMSCs (Figure 4b–d) and improved scaffold-induced osteogenesis. Certain reports have shown that Si and Ca are conducive to the mineralization of preosseous tissue and to the chemotaxis of osteoblasts.[30,31] Moreover, the MBG scaffolds used in the present study presented a macroporous cross-linked structure (Figure 1a), providing a favorable environment for cell and blood vessel penetration.[32−34] In addition, scaffold degradation may provide space and an environment for matrix deposition and tissue growth.

Distribution and Accumulation of ^{45}Ca-MBG Degradation Products in Major Tissues and Organs with Isotopic Tracing. The most important step in assessing the systemic evolution of MBG scaffolds is to determine their distribution and retention in vivo. The distribution and accumulation of ^{45}Ca ions released from MBG scaffolds in tissues and organs were measured by LSC at day 1 and week 1, 4, 8, and 12 after implantation. The results illustrated the systemic distribution and destination of the degradable scaffolds at the implantation site and showed that ^{45}Ca was mainly distributed in the blood and organs, including the heart, lungs, liver, spleen, kidneys, large intestine, small intestine, cerebrum, and cerebellum (Figure 7a). The radioactivity peaked at week 1 and then declined gradually as the scaffolds degraded. There are two possible reasons for this finding: one is that the blood dissolved the scaffolds at an early stage after implantation and the other is that the biodegradation characteristics of MBG (i.e., its mesoporous structure) promoted accelerated ion release.[27] With the gradual formation of new bone, the rate of scaffold degradation decreased at 1 week after implantation, and the concentration of Ca ions dramatically declined in the blood and

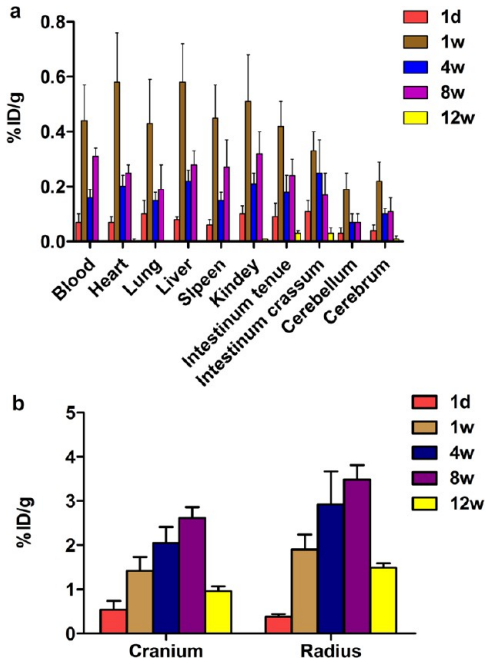

Figure 7. Long-term quantitative tissue distribution of ^{45}Ca-MBG scaffolds. Distribution in (a) blood, heart, lung, liver, kidney, spleen, intestinum tenue, intestinum crassum, cerebrum, and cerebella over 12 weeks and (b) radius and cranium over 12 weeks. The tissue distribution is expressed as the percentage of the implanted dose per gram of tissue (%ID/g), and the data are shown as the mean ± SD ($n = 5$).

various organs. Interestingly, the ^{45}Ca radioactivity at week 8 was slightly higher than that at week 4 in the blood and organs, including the heart, lungs, liver, spleen, small intestine, and kidneys. This increase might be related to the metabolic balance of the organism. The scaffolds continued to degrade, which increased levels of ionic products that accumulated in systemic organs, and the cumulative Ca ions took time to be cleared. In addition, a certain amount of ^{45}Ca was retained in heart at 8 weeks. The accumulation in the heart may be explained by the fact that the heart is the central organ driving blood perfusion and ^{45}Ca in the blood may be captured by the heart through the systemic circulation during the scaffold degradation period. The ^{45}Ca radioactivity was virtually undetectable in the blood and most organs at week 12, indicating that the risk of using MBG scaffolds in vivo could significantly decrease over time. Meanwhile, long-term quantitative tracing of ^{45}Ca in the radius and cranium (Figure 7b) indicated that radioactivity could be detected in these bones at the first time point (24 h postimplantation). The radioactivity in the bone gradually

dx.doi.org/10.1021/am4056886 | ACS Appl. Mater. Interfaces 2014, 6, 3528−3535

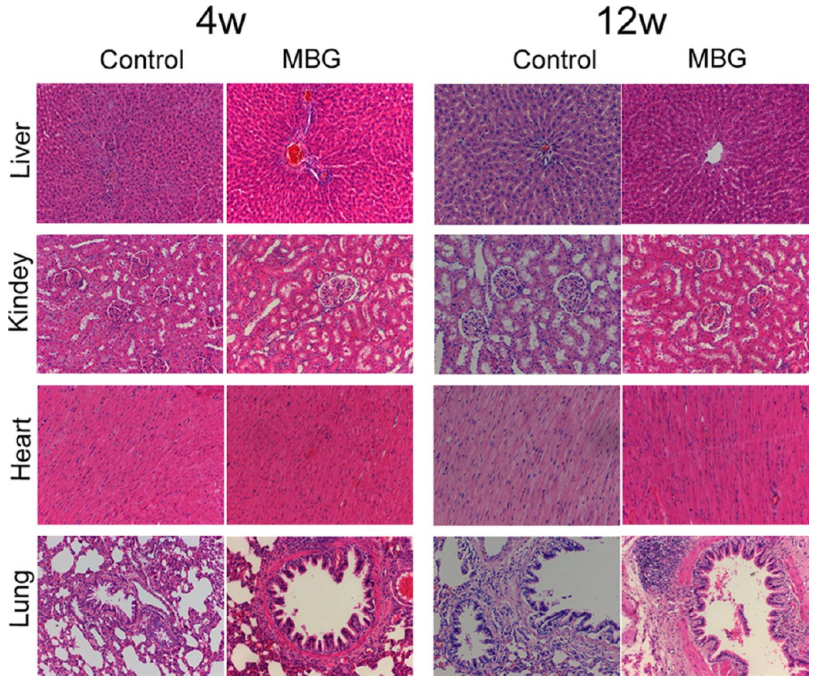

Figure 8. Representative sections from rat tissues after implantation with MBG scaffolds at 4 and 12 weeks. All sections were stained with H&E and observed under a light microscope at 200× magnification. Sham operations were used as the control. No obvious pathological changes were found in the organs after implantation.

Table 3. Effect of MBG Scaffolds on Selected Clinical Hematological Parameters[a]

	4 weeks		12 weeks	
parameters	control	MBG	control	MBG
WBC (10^9/L)	8.48 ± 1.53	7.36 ± 1.05	7.87 ± 0.35	12.9 ± 2.21[a]
LYM (%)	66.20 ± 5.93	72.12 ± 10.39	64.57 ± 1.07	69 ± 3.41
MONO (%)	2.60 ± 0.32	2.68 ± 0.20	2.68 ± 0.31	2.96 ± 0.52
NEU (%)	31.20 ± 5.98	25.20 ± 10.50	32.83 ± 0.96	27.83 ± 3.78
RBC (10^{12}/L)	7.18 ± 0.24	7.67 ± 0.19	7.69 ± 0.27	7.83 ± 0.21
HGB (g/L)	142.40 ± 4.04	152.20 ± 4.82	145 ± 3.24	142.4 ± 1.34
PLT (10^9/L)	732.40 ± 58.12	762.80 ± 73.40	743.4 ± 58.56	725.33 ± 103.71

[a] $p < 0.05$, significantly different.

increased over time and reached a peak at week 8. In addition, the radioactivity in the bone was much higher than in other organs. The main reason for this might be that bone, which is the primary tissue for Ca-ion deposition, has a specific ability for Ca absorption.[35] Our results confirmed once again that the Ca ions released from degraded products into the blood can be easily deposited into bone tissue.

Assessment of the Risk Posed by Degradation Products from MBG Scaffold Evolution. Given that the degradation products of the MBG scaffold can systemically distribute and accumulate in major organs and tissues within 12 weeks, it was necessary to investigate the effect of these products on tissues and organs and to evaluate their biological safety. Our results confirmed there were no obvious pathological changes in the tissue and organs at 4 and 12 weeks after implantation; histological sections of important organs, including the heart, liver, lungs, and kidneys, are shown in Figure 8. There were no abnormalities in blood chemistry indexes, such as ALT, AST, and BUN (data not shown), which indicated that the function of organs, including the liver and kidney, was uninfluenced by implantation. However, hematological testing at 12 weeks (Table 3) showed that the WBC was $(12.9 \pm 2.21) \times 10^9$/L in the experimental group, which was higher than the value of $(7.87 \pm 0.35) \times 10^9$/L in the control group, possibly because phagocytic cells engulfed the degradation products and became activated. These cells may have released proinflammatory cytokines, chemokines, degradative enzymes, reactive oxygen species, and other substances that could cause systemic aseptic inflammation,[31] which is a normal defense mechanism in organisms. The results show that the degradation products of MBG scaffolds, which accumulate in major organs such as the liver and kidney in the short term, do not have a negative biological effect on the morphology or function of tissue. Consequently, MBG scaffolds have good biological safety for clinical application.

CONCLUSIONS

This study has successfully created an effective technology for the ^{45}Ca labeling of porous MBG scaffolds. Using a quantitative tracer, a series of experiments on the long-term evolution of MBG scaffolds in vivo were performed. The results demonstrated that after scaffold implantation in rat femoral condyles the mesoporous structure can accelerate ion exchange at the local level. Additionally, the microenvironment, which is

dx.doi.org/10.1021/am4056886 | ACS Appl. Mater. Interfaces 2014, 6, 3528−3535

formed by reactive ions (mainly Si and Ca ions) released from the MBG scaffolds, facilitates the osteogenic differentiation of rBMSCs in vitro and bone regeneration in vivo. However, the research indicated that only a small amount of Ca ions (less than 9.63%) released during degradation could be directly integrated into new bone matrix. Most ^{45}Ca was distributed and retained in the heart, lungs, spleen, kidneys, intestines, and brain through blood circulation. Moreover, ^{45}Ca accumulated in distal bone tissue, including the radius and cranium. However, the ^{45}Ca radioactivity decreased drastically or disappeared by week 12, and the Ca accumulation did not cause abnormal histopathological changes. All of these findings provide information that is important for a comprehensive understanding of the in vivo evolution of MBG scaffolds. This study preliminarily addresses the benefits and risks of future clinical applications of MBG scaffolds and provides a critical scientific basis for the application of the mesoporous material in bone repair and bone tissue engineering.

AUTHOR INFORMATION

Corresponding Author

*E-mail: jiaosun59@yahoo.com. Tel.:+86 21 63034903. Fax: +86 21 63011643.

Notes

The authors declare no competing financial interest.

ACKNOWLEDGMENTS

This work was supported by grants from the Major Program of the National Natural Science Foundation of China (81190132), the National Key Technology R&D Program (2012BAI22B01), and the Shanghai Sci-Tech Committee Foundation (13DZ2291100).

REFERENCES

(1) Yan, X.; Huang, X.; Yu, C.; Deng, H.; Wang, Y.; Zhang, Z.; Qiao, S.; Lu, G.; Zhao, D. *Biomaterials* **2006**, *27*, 3396−3403.

(2) Wu, C.; Zhou, Y.; Xu, M.; Han, P.; Chen, L.; Chang, J.; Xiao, Y. *Biomaterials* **2013**, *34*, 422−433.

(3) Vallet-Regí, M.; Izquierdo-Barba, I.; Colilla, M. *Philos. Trans. R. Soc., A* **2012**, *370*, 1400−1421.

(4) Vallet-Regí, M.; Balas, F.; Arcos, D. *Angew. Chem., Int. Ed.* **2007**, *46*, 7548−7558.

(5) Huang, S.; Kang, X.; Cheng, Z.; Ma, P.; Jia, Y.; Lin, J. *J. Colloid Interface Sci.* **2012**, *387*, 285−291.

(6) Su, J.; Cao, L.; Yu, B.; Song, S.; Liu, X.; Wang, Z.; Li, M. *Int. J. Nanomed.* **2012**, *7*, 2547−2555.

(7) Gunawidjaja, P. N.; Izquierdo-Barba, I.; Mathew, R.; Jansson, K.; García, A.; Grins, J.; Arcos, D.; Vallet-Regí, M.; Edén, M. *J. Mater.Chem.* **2012**, *22*, 7214−7223.

(8) Yun, H. S.; Park, J. W.; Kim, S. H.; Kim, Y. J.; Jang, J. H. *Acta Biomater.* **2011**, *7*, 2651−2660.

(9) Wu, C.; Zhou, Y.; Fan, W.; Han, P.; Chang, J.; Yuen, J.; Zhang, M.; Xiao, Y. *Biomaterials* **2012**, *33*, 2076−2085.

(10) Alcaide, M.; Portolés, P.; López-Noriega, A.; Arcos, D.; Vallet-Regí, M.; Portolés, M. T. *Acta Biomater.* **2010**, *8*, 892−899.

(11) Wang, C.; Lin, K.; Chang, J.; Sun, J. *J. Biomed. Mater. Res., Part A.* [Online early access]. DOI: 10.1002/jbm.a.34880. Published Online: Aug 2, **2013**.

(12) Wu, C.; Zhou, Y.; Lin, C.; Chang, J.; Xiao, Y. *Acta Biomater.* **2012**, *8*, 3805−3815.

(13) Xie, G.; Wang, C.; Sun, J.; Zhong, G. *Toxicol. Lett.* **2011**, *205*, 55−61.

(14) De Jong, W. H.; Hagens, W. I.; Krystek, P.; Burger, M. C.; Sips, A. J. A. M.; Geertsma, R. E. *Biomaterials* **2008**, *29*, 1912−1919.

(15) Wennerberg, A.; Jimbo, R.; Allard, S.; Skarnemark, G.; Andersson, M. *Int. J. Oral Maxillofac. Implants* **2011**, *26*, 1161−1166.

(16) López-Noriega, A.; Arcos, D.; Izquierdo-Barba, I.; Sakamoto, Y.; Terasaki, O.; Vallet-Regí, M. *Chem. Mater.* **2006**, *18*, 3137−3144.

(17) Izquierdo-Barba, I.; Arcos, D.; Sakamoto, Y.; Terasaki, O.; López-Noriega, A.; Vallet-Regí, M. *Chem. Mater.* **2008**, *20*, 3191−3198.

(18) Kumar, R.; Roy, I.; Ohulchanskky, T. Y.; Vathy, L. A.; Bergey, E. J.; Sajjad, M.; Prasad, P. N. *Acs Nano* **2010**, *4*, 699−708.

(19) Guerquin-Kern, J.-L.; Romer, W.; Wu, T.; Duchambon, P.; Amessou, M.; Carrez, D.; Johannes, L. *Appl. Surf. Sci.* **2006**, *252*, 6925−6930.

(20) *ISO 10993-12. Biological Evaluation of Medical Devices − Part 12: Sample Preparation and Reference Materials*; Report from the International Organization for Standardization: Geneva, Switzerland, 2012.

(21) Wang, C.; Lin, K.; Chang, J.; Sun, J. *Biomaterials* **2013**, *34*, 64−77.

(22) *ISO 10993-11. Biological Evaluation of Medical Devices − Part 11: Test for Systemic Toxicity*; Report from the International Organization for Standardization: Geneva, Switzerland, 2006.

(23) Miao, G.; Chen, X.; Dong, H.; Fang, L.; Mao, C.; Li, Y.; Li, Z.; Hu, Q. *Mater. Sci. Eng., C* **2013**, *33*, 4236−4243.

(24) Wu, C.; Fan, W.; Zhu, Y.; Gelinsky, M.; Chang, J.; Cuniberti, G.; Albrechtf, V.; Friisb, T.; Xiao, Y. *Acta Biomater.* **2011**, *7*, 3563−3572.

(25) Zhang, Q.; Xie, H.; Zhang, Y.; Yu, C.; Chen, W. *Cell Biochem. Biophys.* **2012**, *62*, 119−123.

(26) Wu, C.; Ramaswamy, Y.; Zhu, Y.; Zheng, R.; Appleyard, R.; Howard, A.; Zreiqat, H. *Biomaterials* **2009**, *30*, 2199−2208.

(27) Le Huec, J. C.; Clement, D.; Brouillaud, B.; Barthe, N.; Dupuy, B.; Foliguet, B.; Basse-Cathalinat, B. *Biomaterials* **1998**, *19*, 733−738.

(28) Maeno, S.; Niki, Y.; Matsumoto, H.; Morioka, H.; Yatabe, T.; Funayama, A.; Toyama, Y .; Taguchi, T .; Tanaka, J. *Biomaterials* **2005**, *26*, 4847−4855.

(29) Fei, L.; Wang, C.; Xue, Y.; Lin, K.; Chang, J.; Sun, J. *J. Biomed. Mater. Res., Part B* **2012**, *100*, 1237−1244.

(30) Chai, Y.; Carlier, A.; Bolander, J.; Roberts, S. J.; Geris, L.; Schrooten, J.; Oosterwyck, H. V.; Luyten, F. P. *Acta Biomater.* **2012**, *8*, 3876−3887.

(31) Ren, P. G.; Lee, S. W.; Biswal, S.; Goodman, S. B. *Biomaterials* **2008**, *29*, 4760−4765.

(32) Karageorgiou, V.; Kaplan, D. *Biomaterials* **2005**, *26*, 5474−5491.

(33) Hoppe, A.; Güldal, N. S.; Boccaccini, A. R. *Biomaterials* **2011**, *32*, 2757−2774.

(34) Claase, M. B.; de Bruijn, J. D.; Grijpma, D. W.; Feijen, J. *J. Mater. Sci.: Mater. Med.* **2007**, *18*, 1299−1307.

(35) Charoenphandhu, N.; Krishnamra, N. *Can. J. Physiol. Pharmacol.* **2007**, *85*, 569−581.